Developmental and Comparative Immunology 130 (2022) 104352

Contents lists available at ScienceDirect

Developmental and Comparative Immunology

journal homepage: www.elsevier.com/locate/devcompimm

# A flow cytometry based approach to identify distinct coelomocyte subsets of the purple sea urchin, *Strongylocentrotus purpuratus*

Megan A. Barela Hudgell, Leon Grayfer, L. Courtney Smith *

*Department of Biological Sciences, George Washington University, Washington, DC, 20052, USA*

ARTICLE INFO

*Keywords:*
Invertebrate
Immune cells
Flow cytometry
Echinoderm
Phagocytes
Vibratile cells
Colorless spherule cells
Red spherule cells

ABSTRACT

The sea urchin, *Strongylocentrotus purpuratus*, possesses at least seven distinguishable cell populations in the coelomic fluid, which vary in morphology, size, and function. Of these, the large phagocytes, small phagocytes, and red spherule cells are thought to be key to the echinoid immune response. Because there are currently no effective and rapid means of evaluating sea urchin coelomocytes, we developed a flow cytometry based approach to identify these subsets from unseparated, unstained, live cells. In particular our gating strategy distinguishes between the large phagocytes, small phagocytes, red spherule cells, and a mixed population of vibratile cells and colorless spherule cells. This flow cytometry based analysis increases the speed and improves the reliability of coelomocyte analysis compared to differential cell counts by microscopy.

## 1. Introduction

The coelomocytes, or immune cells, of echinoids are found predominantly in the coelomic fluid (CF) that fills the internal body cavity, although many of these cells are present in, and wander through the tissues of these animals (Hyman, 1955). Coelomocytes have been identified in the gut, the pharynx, the gonads, and the axial organ (Dheilly et al., 2011; Majeske et al., 2013b; Golconda et al., 2019). Elevated expression of conserved hematopoietic gene regulatory networks in the axial organ and the pharynx infers that these are the sites of coelomocyte proliferation, differentiation, and the release into the CF in adult echinoids (Golconda et al., 2019). Coelomocytes vary in size, morphology, and function (Johnson, 1969; Chia and Xing, 1996) with three major categories defined as phagocytes, spherule cells, and vibratile cells (reviewed in (Smith et al., 2018)). The phagocyte class of coelomocytes is composed of four subsets of cells based on their size and cytoskeletal structure. There are two types of large phagocytes (20–50 μm), which are differentiated based on their cytoskeletal morphology when spread on glass (Edds, 1977, 1979, 1993; Henson et al., 1992, 1999). The discoidal phagocytes have a disc-like or fried egg morphology with radial orientation of the actin filaments, whereas the polygonal phagocytes spread on glass into a polygon form with actin filaments aligned across the cell. In addition, medium phagocytes are intermediate in size (20–30 μm) with an unusual pentagonal or hexagonal shape when spread on glass and were first noted in sea urchins undergoing coelomocyte replacement after experimental depletion of the CF (Golconda et al., 2019). The fourth morphotype, small phagocytes, are significantly smaller (3–10 μm) than the other classes of phagocytes and show filopodial morphology when spread on glass (Clow et al., 2000; Gross et al., 2000; Golconda et al., 2019), however they appear in spherical morphology in suspension (Oren et al., 2019). Although this description of the phagocyte class of coelomocytes is based strictly on morphology and size, it is likely that these subsets may have additional differences based on function, as suggested by differences in immune protein expression and secretion, including the complement C3 homologue, SpC3 (Gross et al., 2000; Clow et al., 2004), and the SpTransformer proteins (Brockton et al., 2008; Chou et al., 2018).

There are two types of spherule cells, characterized by the large cytoplasmic spherules or vesicles that are either red or colorless (Johnson, 1969; Smith, 1981; Service and Wardlaw, 1984); reviewed in (Smith et al., 2018)). Red spherule cells (RSCs; 8–20 μm) are amoeboid on glass and contain echinochrome A in their cytoplasmic vesicles. Echinochrome A is a red 1,4-napthoquinone pigment (Coates et al., 2017) that imparts auto-fluorescence to the RCSs, which has been employed to distinguish these cells by flow cytometry and cell sorting (Oren et al., 2019; Hira et al., 2020). The colorless spherule cells (CSCs), which are of similar size and morphology as the RSCs, are also amoeboid but do not produce echinochrome A or other pigments. Vibratile cells (5–10 μm) maintain a spherical shape with an irregular nucleus and many cytoplasmic vesicles, and each has a characteristic single long

* Corresponding author.
*E-mail address:* csmith@gwu.edu (L.C. Smith).

https://doi.org/10.1016/j.dci.2022.104352
Received 8 December 2021; Received in revised form 12 January 2022; Accepted 14 January 2022
Available online 20 January 2022

**Table 1**
Density centrifugation gradients used to separate different coelomocyte types.

| *Gradient type* | [a] | *Fraction* | | | | | *Reference* |
|---|---|---|---|---|---|---|---|
| | | 1 | 2 | 3 | 4 | 5 | |
| Percoll Step Gradient | 5 | Debris only, no cells | Polygonal phagocytes | Discoidal phagocytes | Vibratile cells and CSCs[b] | RSCs[c] | Smith et al. (1992) |
| Continuous Percoll Gradient | 4 | Polygonal and Discoidal phagocytes | Vibratile cells | CSCs | RSCs | N/A[d] | Coates et al. (2017) |
| Iodixanol Step Gradient | 5 | Polygonal phagocytes | Discoidal phagocytes | Vibratile cells | CSCs | RSCs | (Gross et al., 2000; Arizza et al., 2007; Liao and Fugmann, 2017) |
| Sodium Metrizoate Step Gradient | 3 | Polygonal and Discoidal phagocytes | Vibratile and CSCs | RSCs | N/A | N/A | (Bertheussen and Seljelid, 1978; Pagliara and Canicattì, 1993) |
| Triosil and Ficoll mix | 4 | Vibratile cells | Large phagocytes | CSCs | RSCs | N/A | Messer & Wardlaw (1980) |
| Sucrose Gradient | 2 | Discoidal phagocytes | Polygonal phagocytes | N/A | N/A | N/A | Edds (1993) |

[a] Number of cell fractions collected from the gradient.
[b] CSCs, colorless spherule cells.
[c] RSCs, red spherule cells.
[d] N/A, not applicable, the step is not included in the gradient.

flagellum (reviewed in (Chia and Xing, 1996; Smith et al., 2018)). The flagellar activity has been hypothesized to move these cells about the CF (Smith, 1981; Chia and Xing, 1996), although the functional importance of this activity is not known. All seven of these coelomocyte types show varying morphologies and sizes, and when observed in suspension most cell types are generally reported as about the same size compared to when observed on glass slides (Johnson 1969; reviewed in Smith et al., 2018). However, the large phagocytes appear smaller in suspension than after they have spread into essentially two dimensions on glass. Because all cell types are present in the CF, they can be collected easily for evaluation without sacrificing the animal (see (Smith et al., 2019)).

Percoll density gradients, microscopy, and cell staining have been used to understand the dynamic characteristics and functions of different coelomocyte populations (Johnson, 1969; Yui and Bayne, 1983; Smith et al., 1992; Brockton et al., 2008). A variety of density gradients have been used to separate coelomocytes into different cell types (reviewed in (Chia and Xing, 1996)) although these methods can be limited. Both step and continuous Percoll gradients (Smith et al., 1992; Coates et al., 2017), step gradients of iodixanol (Gross et al., 2000; Arizza et al., 2007; Liao and Fugmann, 2017), sodium metrizoate (Bertheussen and Seljelid, 1978), a mixture of triosil and ficoll (Messer and Wardlaw, 1980), and sucrose (Edds, 1993) have all been used with varying levels of success to separate different coelomocyte types (Table 1). While step gradients have enabled the evaluation of different coelomocyte types, these approaches are imperfect because fractions that are enriched for a particular coelomocyte are typically contaminated with other cell types (Gross et al., 2000). Furthermore, density fractionation has the potential problem of coelomocyte loss during the separation procedure. Hence, while useful, these methods are not adequate to quantify changes in coelomocyte populations among sea urchins or in an individual animal over time.

Flow cytometry is an alternative approach for evaluating invertebrate immune cells, as reported for sea urchins (Liao and Fugmann, 2017; Piryaei et al., 2018; Monte et al., 2019; Oren et al., 2019; Smith et al., 2019; Hira et al., 2020), a sea star (Andrade et al., 2021), a clam (Brousseau et al., 2000), and an earthworm (Engelmann et al., 2016). In general, flow cytometry gates to identify coelomocytes from echinoids tend to show cell populations that are heterogeneous and defined based on the gates rather than cell types, and fail to establish gates for all different cell types. To improve on this approach, we report an optimized gating strategy for flow cytometry that separates and defines several types of coelomocytes from the California purple sea urchin, *Strongylocentrotus purpuratus*. Gate optimization is based on different cell fractions that are enriched by Percoll step density centrifugation and verified by microscopy. Gates established based on cell fractions are subsequently employed to analyze unseparated, unstained, live coelomocytes. These gates distinguish large phagocytes, small phagocytes, RSCs, and a mixture of vibratile cells and CSCs. It is noteworthy that neither density centrifugation nor flow cytometry could separate vibratile cells and CSCs. This coelomocyte gating approach can be employed in future work to evaluate changes in distinct cell populations over time and/or in response to experimental manipulations.

## 2. Methods

### 2.1. Sea urchin care

Sea urchins were collected from the nearshore waters of the Pacific Ocean off the coast of southern California and purchased from Marinus Scientific (Long Beach, CA) or the Southern California Sea Urchin Company (Corona del Mar, CA). Animals were maintained as described (Gross et al., 2000) and fed once a week with re-hydrated kelp (*Saccharina japonica*, Wel-Pac Dashi Kombu). Sea urchins were housed for up to two years in 125 gallon re-circulating marine aquaria.

### 2.2. Coelomocyte collection

CF (50–400 μL) was withdrawn from animals with a 23 gauge, ¾ inch needle attached to a 1 mL syringe that was inserted through the sea urchin peristomial membranes at about a 45° angle, and into the coelomic or body cavity (see (Smith et al., 2019)). To prevent clotting, the syringe was prefilled with ice cold anticoagulant composed of calcium- and magnesium-free seawater (CMFSW-EH; 460 mM NaCl, 10.73 mM KCl, 7.04 mM $Na_2SO_4$, 2.38 mM $NaHCO_3$, 70 mM EDTA, 20 mM HEPES pH 7.4 (Majeske et al., 2013a)) that was at least equal to the volume of the CF that was withdrawn. In some cases, CF was withdrawn and the volume was adjusted to 1 mL with additional cold CMFSW-EH prior to expelling the diluted CF into a 1.5 mL tube on ice. The diluted CF was held on ice for up to 1 h prior to further use. Coelomocytes were counted with a TC20 automatic cell counter (BioRad) according to Chou et al. (2018). The original coelomocyte concentration in the CF was calculated based on the cell count and the CF dilution factor into CMFSW-EH.

### 2.3. Cell separation by discontinuous percoll density gradient centrifugation

Percoll (25 ml; Sigma-Aldrich) was dialyzed overnight against 2 L of CMFSW-EH at 4 °C with slow stirring to remove and chelate divalent cations to block coelomocyte clotting reactions. Dialyzed, ice cold Percoll was diluted with cold CMFSW-EH to 2.5%, 20%, 30%, 50%, and 70% to construct a step gradient on ice as reported previously (Smith

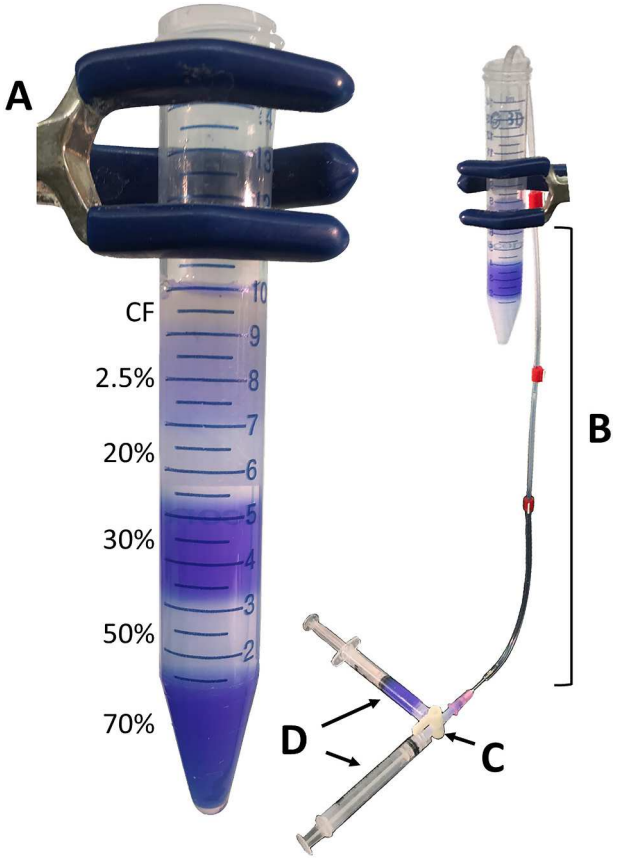


**Fig. 1. Construction of a Percoll step gradient**. (**A**) A Percoll step gradient is shown with the percentages of Percoll identified by the addition of a low concentration of bromophenol blue in alternating layers. The Percoll delivery system used to generate the step gradient is composed of a glass capillary inserted to the bottom of the 15 mL conical centrifuge tube, which is attached to a 1.14 mm PVC double manifold tubing (**B**), and connected to a stopcock (**C**) with a 16 gauge needle. Two syringes (**D**) are inserted into the stopcock containing 1–2 mL of different percentages of Percoll. Increasing percentages of Percoll are delivered from a syringe through the tubing and capillary into the bottom of the centrifuge tube to generate the layers of the step gradient. (For interpretation of the references to color in this figure legend, the reader is referred to the Web version of this article.)

et al., 1992, 2019) (Fig. 1). Each step in the gradient was added to a 15 mL conical tube (Fig. 1A) using a glass capillary (ThermoFisher Scientific product code 981.0114.000) attached to a 1.14 mm PVC double manifold tubing (ThermoFisher Scientific product code 981.0114.000) (Fig. 1B) using a 16gauge needle to connect a three-way stop cock (Fig. 1C) to the tubing. The open end of the capillary was placed at the bottom of the 15 mL conical tube and two 3 ml syringes (Fig. 1D) filled with different concentrations of Percoll were attached to the stop cock. Each Percoll step (1–2 mL) was delivered slowly to the bottom of the 15 mL conical tube via the capillary starting with the 2.5% and followed by under-layering each subsequently higher percentage of Percoll to result in discrete interfaces between Percoll layers (Fig. 1A). The use of this delivery system avoided introducing air bubbles into the gradient that would disrupt the interfaces when ascending to the surface.

Between $10^4$ and $10^6$ cells in 1 mL were layered over the 2.5% Percoll step using a pasture pipette. The gradient was centrifuged immediately at 250×*g* for 15 min at 4 °C in a swinging bucket rotor with a slow start and no brake. The cells that accumulated at the interfaces of the Percoll density steps were unloaded from the top to the bottom by aspiration with pasture pipettes and delivered into separate 15 mL conical tubes on ice that were prefilled with 5–15 mL of CMFSW-EH. These cell fractions were pelleted at 400 - 500×*g* for 15 min at 4 °C. The cell pellets were resuspended in 200–500 μL of CMFSW-EH and kept on ice prior to further evaluation.

### 2.4. Preparation of Vibrio diazotrophicus

*Vibrio diazotrophicus* (American Type Culture Collection; item #33466) (Guerinot et al., 1982) was grown over night at room temperature in marine broth (MB; 3.74% MB powder [Difco Laboratories] plus 0.3% yeast extract, 0.5% proteose peptone) as reported (Sherman et al., 2015; Lun et al., 2016; Chou et al., 2018). Bacteria were pelleted and re-suspended in artificial CF (aCF; 10 mM $CaCl_2$, 14 mM KCl, 50 mM $MgCl_2$, 390 mM NaCl, 1.7 mM $NaHCO_3$, 25 mM $Na_2SO_4$ (Terwilliger et al., 2007)). Bacteria were counted on a Petroff Hausser Chamber (Hausser Scientific) and adjusted with aCF to $10^4$ or $10^6$ bacteria/μL. Aliquots (1 mL) of *V. diazotrophicus* were heat-killed at 95 °C for 30 min, verified for lack of growth on a MB plate according to Sherman et al. (2015) and stored at −20 °C.

### 2.5. Immune stimulation

Sea urchins were injected with either heat-killed *V. diazotrophicus* or aCF (vehicle injury control) through the peristomial membrane and into the coelomic cavity using 26 gauge needles attached to 1 mL syringes. The volume of *V. diazotrophicus* injected was based on the bacterial concentration and the estimated CF volume per animal according to Smith et al. (1995) coelomic fluid (mL) = weight (gm) x 0.22 such that the number of *V. diazotrophicus* cells per ml of CF was consistent across animals of different sizes. The volume of aCF that was injected was adjusted to be equal to the volume of *V. diazotrophicus* that was injected.

CF (50–200 μl) was withdrawn from sea urchins (n = 4) on day 0 prior to any manipulation to establish baseline data. Sea urchins (n = 2) received the first injection of $10^4$ *V. diazotrophicus*/mL of CF in 30 μL of aCF on day 2, which was followed by the second injection of $10^6$ *V. diazotrophicus*/mL of CF in 30 μL of aCF on day 5 according to Majeske et al. (2014) and Sherman et al. (2015). Control animals (n = 2) received injections of 30 μL aCF (vehicle) on the same schedule. CF (50–200 μl) was withdrawn from each animal for cell analysis by flow cytometry at baseline and 1 day after the last injection of either *V. diazotrophicus* or the vehicle control.

### 2.6. Flow cytometry

Coelomocytes diluted in CMFSW-EH from individual sea urchins were incubated with propidium iodide (PI; 1 μg/mL) on ice for 5 min and evaluated by flow cytometry as described (Smith et al., 2019) using an Accuri C6 Flow Cytometer (BD Biosciences) to identify the different subsets of coelomocytes. At least $10^5$ total coelomocyte events were recorded for flow cytometry data and parameters were established for each gate as described in detail below. Data were analyzed using FlowJo™ (v10.6.2) software (BD Biosciences https://www.flowjo.com).

## 3. Results

### 3.1. Enriched populations of coelomocytes enable an optimized flow cytometry gating strategy

A flow cytometry gating strategy to analyze sea urchin coelomocytes based on analyses of size vs. internal complexity has been reported (Smith et al., 2019). Staining cells with antibodies to the SpTransformer (SpTrf) proteins has been used to identify and sort small phagocytes, and red auto-fluorescence of echinochrome A has been employed as a gating strategy to sort RSCs (Coates et al., 2017; Oren et al., 2019; Smith et al., 2019; Hira et al., 2020). Flow cytometry has been used in conjunction with fluorescently labeled lectins to identify different types of coelomocytes, although this approach demonstrated that specific lectins are often present on multiple types of cells (Liao and Fugmann, 2017). Two

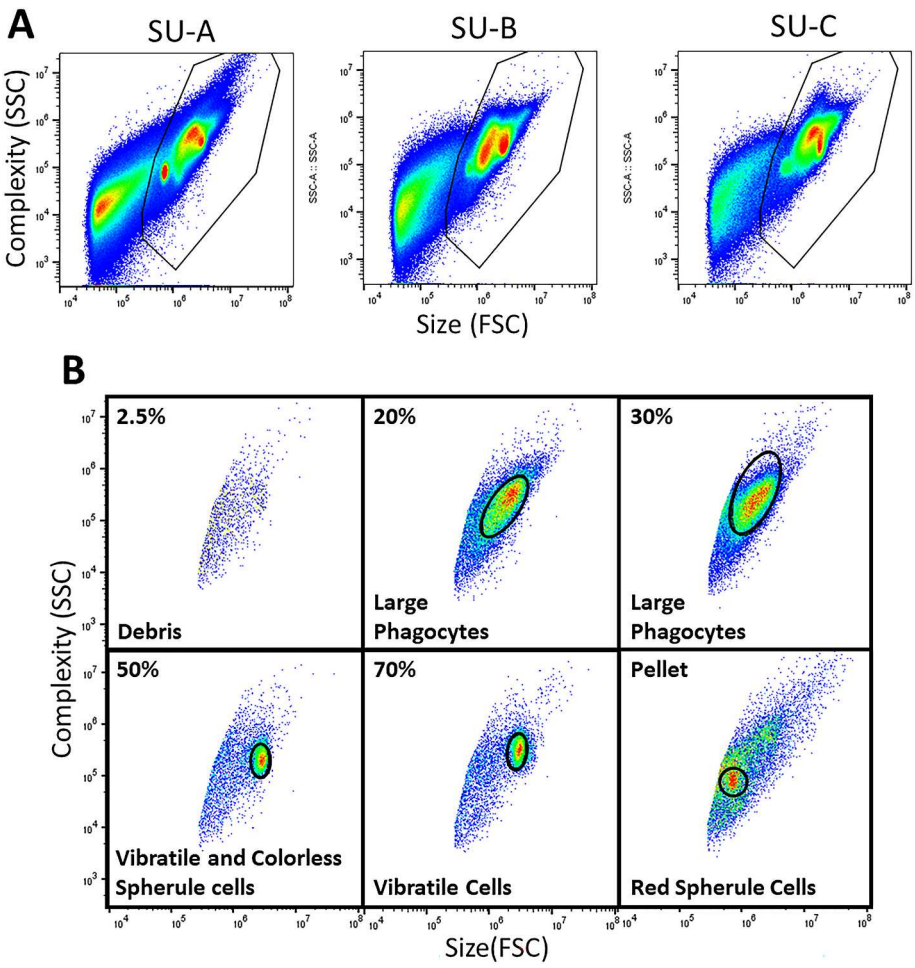


**Fig. 2. Gates for populations of coelomocyte types are based on cell separation by Percoll step density gradient.** (**A**) The polygon gate distinguishes all coelomocytes from debris in CF from three sea urchins (SU-A, -B, –C). This gate is described in (Smith et al., 2019) and employed here. (**B**) Coelomocyte fractions from Percoll step gradient density centrifugation are based on results from three sea urchins (see Fig. S1) and used to optimize distinct gates for each cell population. Representative scatter plots in log scale for internal complexity vs. size (SSC-A vs. FSC-A) for each cell fraction are identified by black circles and ovals that indicate the positions of the majority cell population from each Percoll layer. Areas of cell density range from high (red), medium (green), and low (blue) and correlate with cells that range from similar to dissimilar size and complexity. (For interpretation of the references to color in this figure legend, the reader is referred to the Web version of this article.)

monoclonal antibodies raised against coelomocytes have been used in flow cytometry to evaluate large phagocytes as well as another coelomocyte type with many cytoplasmic vesicles (Wang et al., 2018). Although these approaches are noteworthy, they either fail to identify all types of coelomocytes or are designed to target only specific cell types for which reagents are available. Consequently, we developed a gating strategy to identify as many distinct populations of coelomocytes as possible based on the characteristics of unlabeled or minimally labeled live cells. To correlate distinguishable populations in the flow cytometry scatter plots to specific cell subsets, CF was collected from three sea urchins (SU-A, -B, –C) and cell types were separated by centrifugation through Percoll density step gradients (Fig. 1) as described (Smith et al., 1992, 2019). Fractions enriched for specific coelomocyte types were verified by microscopy prior to analysis by flow cytometry and were consistent with previous descriptions.

The initial analysis of coelomocyte fractions by flow cytometry employed a preliminary gating strategy based on previous studies (see Fig. 4 in (Smith et al., 2018)) that assessed cellular complexity vs. size (side scatter - area [SSC-A] vs. forward scatter - area [FSC-A]). Coelomocytes from three sea urchins were used because of variations in coelomocyte populations among animals that has been reported previously (Brockton et al., 2008; Golconda et al., 2019). The placement of the gate for total coelomocyte populations was optimized on the scatter plots based on the variability of each cell type (Fig. 2A). This initial gate was also used to exclude debris from further consideration. Because this initial gate for total coelomocytes did not identify specific cell types in the scatter plot, coelomocytes were separated by density centrifugation into cell fractions that were confirmed to cell type by microscopy followed by flow cytometry analyses of the fractions. As reported previously (Majeske et al., 2014; Smith et al., 2019), the 2.5% Percoll layer separated non-cellular components from coelomocytes that were generally not present in this layer (Fig. 2B). In agreement with previous reports (Smith et al., 2019), the 20% Percoll layer contained polygonal phagocytes, which were identified in the scatter plots by an oval gate that defined this population of large cells with variable complexity (Fig. 2B, S1). The 30% Percoll layer contained discoidal phagocytes that overlapped with the polygonal phagocytes on the scatter plots, indicating that these two cell types were of similar size and complexity, which was consistent with evaluation by microscopy. Although the polygonal phagocytes exhibited slightly less granularity (side scatter) than the discoidal phagocytes, these differences were not sufficient to separate these two cell populations into different gates by flow cytometry. Hence, these two cell types were gated together as the large phagocyte population.

The 50% Percoll layer contained a mixture of vibratile cells and CSCs that were not separated by Percoll. These two cell types also appeared together in the scatter plot in a small area, indicating that these respective populations were very similar in size and granularity. The 70% layer contained only vibratile cells (Fig. 2B, S1), which were slightly larger than the CSCs. Given that the vibratile cells and CSCs could not be separated consistently by either Percoll density centrifugation or reliably distinguished by flow cytometry, they were analyzed together in one gate. The RSCs passed through all layers of the Percoll gradient and formed a pellet. These cells were slightly smaller than the vibratile cells and CSCs and although they have been characterized with many large spherules or granules by microscopy (reviewed in (Chia and Xing, 1996; Smith et al., 2018)), they showed low granularity on the scatter plots (Fig. 2B, S1). The scatter plot profiles for this cell type

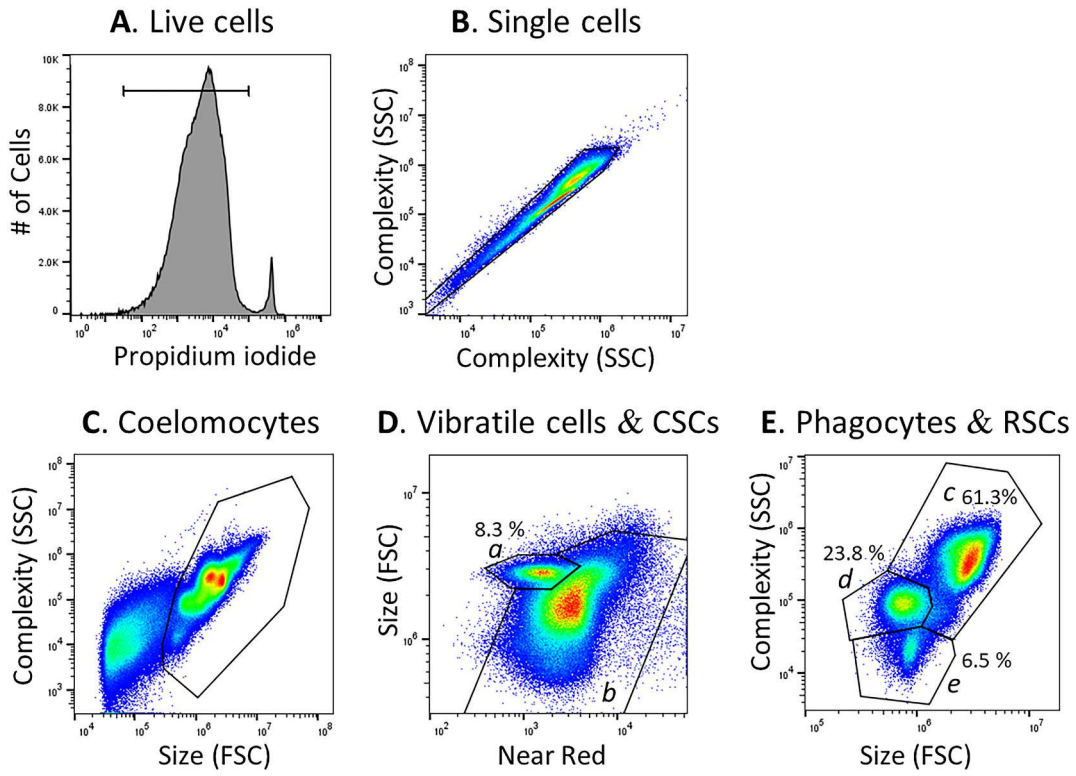


**Fig. 3. Identification of gates to analyze sea urchin coelomocyte populations by flow cytometry**. The scheme used to analyze unfractionated coelomocyte populations to identify different types of coelomocytes shows gates that are specific for different cell types based on their characteristics. (**A**) Live cells are identified by exclusion of dead cells stained with propidium iodide. (**B**) The gate for single events removes instances of two or more cells passing through the flow cytometer at the same time based on SSC-A vs. SSC-H. (**C**) Live coelomocytes of all types are gated based on size vs. internal complexity (FSC-A vs. SSC-A) and removes debris as described (Smith et al., 2019). (**D**) The near red filter for live cells that acquire low levels of PI staining separates the vibratile cells and CSCs (gate *a*) from the other cell populations (gate *b*) based on size (FSC-H) vs. near red (FL3-H). (**E**) Additional gates separate large phagocytes (gate *c*), RSCs (gate *d*), and small phagocytes (gate *e*) based on size vs. internal complexity (FSC-H vs. SSC-H). The percentage of cells in each gate is shown in (**D**) and (**E**) and were calculated based on the total number of events in the plot to adjust for the multiple gating strategy. (For interpretation of the references to color in this figure legend, the reader is referred to the Web version of this article.)

overlapped with the smallest and least granular of the large phagocytes. Small phagocytes were not observed in the preliminary Percoll fractions because these cells are not typically observed in the absence of immune stimuli (Brockton et al., 2008; Golconda et al., 2019). When present, however, small phagocytes tend to be found with the large phagocytes on both 20% and 30% Percoll layers (Majeske et al., 2014). It was therefore impossible to establish a gate for small phagocytes with this approach.

### 3.2. Flow cytometry gating distinguishes distinct coelomocyte subsets

To employ the established gates to assess distinct cell populations in unfractionated coelomocytes, we first excluded $PI^+$ (dead) cells from further analysis (Fig. 3A). Cell doublets and aggregates were gated out using complexity-area vs. complexity-height plots (SSC-A vs. SSC-H) to evaluate only single cells (Fig. 3B). This was followed by excluding any additional debris with a gate that encompassed all coelomocyte types based on size vs. complexity (FSC-A vs. SSC-A), as reported previously (Smith et al., 2019) (Fig. 3C). During the step to exclude dead, $PI^+$ coelomocytes, we observed that, with the exception of the RSCs, all cell types acquired low levels of red fluorescence that was distinguishable from the $PI^+$ cells (Fig. 4). Presently, we do not understand how coelomocytes acquired low levels of PI but we anticipate that this occurred through adsorption to the surface of live cells. Endocytosis of cell surface molecules or uptake of $PI^+$ dying cells or debris by coelomocytes is blocked by calcium ion chelation by EDTA (Chou and Smith, unpublished observation) and therefore was not a source of the low-level red fluorescence. Because all cell types exhibited some overlap in the scatter plots (Fig. 2A), this shift in red fluorescence improved discrimination among distinct cell types because of greater red fluorescence of the large phagocytes (Fig. 4, black circle) resulting in greater scatter separation from the vibratile cells and CSCs (Fig. 4, yellow arrows, brackets). In turn, this greater resolution across coelomocyte populations allowed us to establish a gate specific for vibratile cells and CSCs (Fig. 3D, gate *a*) relative to the other coelomocytes (Fig. 3D, gate *b*). However, the red fluorescence acquired from PI and the shifted location of the large phagocytes, reduced the capacity to distinguish them from the RSCs because of the auto-fluorescence of echinochrome A (Fig. 4, red arrows) (Hira et al., 2020). Therefore, these two cell types were discriminated by gates established using size and complexity parameters (Fig. 3E, gates *c*, *d*). Through the combination of Percoll density centrifugation, microscopy, and a flow cytometry gating strategy, most of the coelomocyte populations in sea urchins could be identified. Furthermore, the percentages of the respective cell populations from the unseparated coelomocytes as identified by flow cytometry (Fig. 3D and E) were consistent with reports of different coelomocyte populations for *S. purpuratus* based on other methods (Johnson, 1969; Smith et al., 1992; Gross et al., 2000; Brockton et al., 2008; Golconda et al., 2019; Oren et al., 2019; reviewed in Smith et al., 2010).

### 3.3. Small phagocytes are identified in sea urchins responding to Vibrio challenge

Coelomocytes from sea urchins that have not been immunologically stimulated typically do not have significant numbers of small phagocytes (Brockton et al., 2008; Golconda et al., 2019). To identify

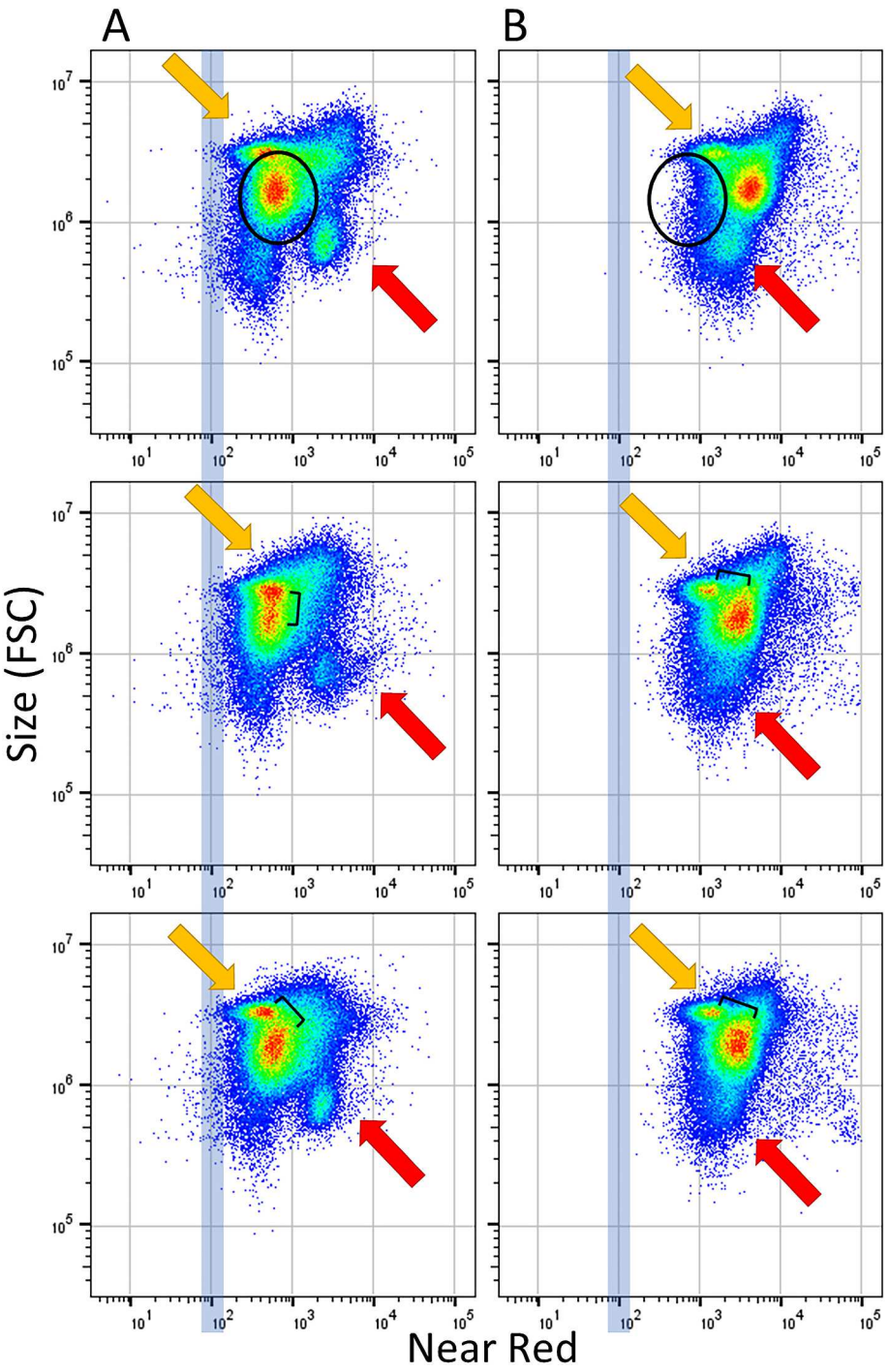


**Fig. 4. Most coelomocyte types acquire low levels of red fluorescence after incubation with PI and shift positions on the scatter plots.** Coelomocytes from three sea urchins are shown after incubation on ice for 5 min without (**A**) and with (**B**) propidium iodide (PI, 1 μg/mL). Scatter plots of coelomocytes are based on size (FSC–H) vs. near red (FL3-H). The mixed population of vibratile cells and CSCs (yellow arrows) are more distinct after incubation with PI (compare brackets) because of the greater shift by large phagocytes (black circles). RSCs (red arrows) become less distinct after incubation with PI. Both changes are relative to the shift of the large phagocytes. (For interpretation of the references to color in this figure legend, the reader is referred to the Web version of this article.)

these cells and to establish a gate for small phagocytes from unseparated coelomocytes, sea urchins were injected twice with heat-killed *Vibrio diazotrophicus*, which is known to induce immune activation (Brockton et al., 2008; Oren et al., 2019). Because small phagocytes appear in Percoll gradients with both types of large phagocytes (Majeske et al., 2014), attempts to identify small phagocytes as separate density fractions prior to flow cytometry were not carried out. Cell populations from these *Vibrio* challenged sea urchins were compared to populations from sea urchins that were injected with aCF (vehicle injury control). Cells of small size and low complexity were not present at baseline but appeared in animals A and B after the challenges with *V. diazotrophicus* (Fig. 5, green arrows). These changes relative to baseline were not evident in animals C and D, which were injected with aCF (Fig. 5). The appearance, size, and characteristics of these cells on scatter plots were consistent with small phagocytes, in agreement with Oren et al. (2019). Similarly, RSCs were also noted to increase in animals A and B (Fig. 5, red arrows) but not in animals C and D, in agreement with previous reports (Brockton et al., 2008; Golconda et al., 2019). The changes in these cell populations in sea urchins injected with *V. diazotrophicus* established a gate for small phagocytes (Fig. 3E, gate *e*) and verified the gate for the RCSs (Fig. 3E, gate *d*).

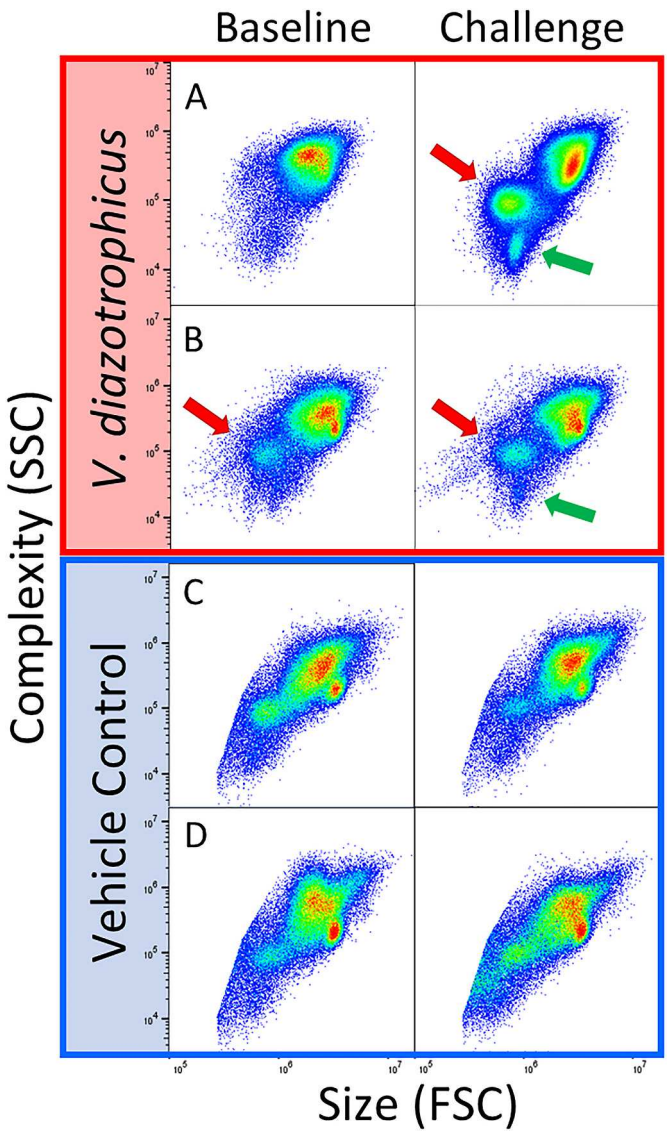


**Fig. 5. Small phagocytes appear in sea urchins responding to *Vibrio diazotrophicus*.** Unseparated coelomocytes collected from four sea urchins (A–D) are evaluated by flow cytometry (FSC-H vs. SSC-H) to compare cell populations before treatment (baseline) and after two injections (challenge) of either *V. diazotrophicus* or aCF (vehicle) as the injection control. Cells of small size and low internal complexity (green arrows) appear in animals A and B but not in animals C and D. RSCs (red arrows) also increase in response to *V. diazotrophicus* (animals A, B) but not in response to vehicle (animals C, D). (For interpretation of the references to color in this figure legend, the reader is referred to the Web version of this article.)

## 4. Conclusions

The gating strategy to characterize coelomocytes from the purple sea urchin follows a workflow of excluding dead cells based on PI uptake (Fig. 3A) followed by gating out cell aggregates (Fig. 3B) and gating for total coelomocytes (Fig. 3C). Two gates, comparing cellular complexity and near red fluorescence separate the vibratile cells and CSCs from the rest of the coelomocytes (Fig. 3D, gates *a*, *b*). Finally, the rest of the cells defined by gate *b* are evaluated by size and internal complexity to identify the large phagocytes, the RSCs, and the small phagocytes (Fig. 3E, gates *c*, *d*, *e*). The appearance of the small phagocytes in response to *Vibrio* and their characteristic small size is consistent with several prior reports of these cells (Brockton et al., 2008; Golconda et al., 2019; Oren et al., 2019), and therefore it was not deemed necessary to verify the cells in this gate by sorting, staining, and microscopy. While not all of the different coelomocyte types could be completely distinguished, this gating strategy significantly improves the assessment of four cell populations compared to previous reports for echinoids (Romero et al., 2016; Liao and Fugmann, 2017; Piryaei et al., 2018; Oren et al., 2019; Smith et al., 2019; Hira et al., 2020). This approach can be employed as a starting point for analyzing changes in live cell populations in sea urchins responding to various challenges without the need to spin or settle cells onto slides, fix, and stain them prior to evaluation by microscopy and laborious differential cell counting. Furthermore, only the phagocyte populations tend to stick reliably to glass slides. The flow cytometry gating method reported here has potential to expand the questions that address functions and responses of all coelomocyte types by providing a rapid means to track unstained live coelomocytes over time in vivo, in addition to identifying variations in coelomocyte populations among individual sea urchins.

## Acknowledgements

Animal care was carried out by Caroline R. Reynolds and Chloe G. Shaw. This project was supported by funding from the NSF (IOS-1855747) to LCS and LG, departmental startup funding to LG, and awards from the Wilbur V. Harlan Trust through the Department of Biological Sciences and the George Washington University Columbian College of Arts and Sciences to MABH.

## Appendix A. Supplementary data

Supplementary data to this article can be found online at https://doi.org/10.1016/j.dci.2022.104352.

## References

Andrade, C., Oliveira, B., Guatelli, S., Martinez, P., Simões, B., Bispo, C., Ferrario, C., Bonasoro, F., Rino, J., Sugni, M., Gardner, R., Zilhão, R., Coelho, A.V., 2021. Characterization of coelomic fluid cell types in the starfish *Marthasterias glacialis* using a flow cytometry/imaging combined approach. Front. Immunol. 12, 641664 https://doi.org/10.3389/fimmu.2021.641664.

Arizza, V., Giaramita, F.T., Parrinello, D., Cammarata, M., Parrinello, N., 2007. Cell cooperation in coelomocyte cytotoxic activity of *Paracentrotus lividus* coelomocytes. Comp. Biochem. Physiol. Mol. Integr. Physiol. 147, 389–394. https://doi.org/10.1016/j.cbpa.2007.01.022.

Bertheussen, K., Seljelid, R., 1978. Echinoid phagocytes in vitro. Exp. Cell Res. 111, 401–412. https://doi.org/10.1016/0014-4827(78)90185-4.

Brockton, V., Henson, J.H., Raftos, D.A., Majeske, A.J., Kim, Y., Smith, L.C., 2008. Localization and diversity of 185/333 proteins from the purple sea urchin – unexpected protein-size range and protein expression in a new coelomocyte type. J. Cell Sci. 121, 339–348. https://doi.org/10.1242/jcs.012096.

Brousseau, P., Pellerin, J., Morin, Y., Cyr, D., Blakley, B., Boermans, H., Fournier, M., 2000. Flow cytometry as a tool to monitor the disturbance of phagocytosis in the clam *Mya arenaria* hemocytes following in vitro exposure to heavy metals. Toxicology 142, 145–156. https://doi.org/10.1016/s0300-483x(99)00165-1.

Chia, F.S., Xing, J., 1996. Echinoderm coelomocytes. Zool. Stud. 35, 231–254.

Chou, H., Lun, C.M., Smith, L.C., 2018. SpTransformer proteins from the purple sea urchin opsonize bacteria, augment phagocytosis, and retard bacterial growth. PLoS One 13, e0196890. https://doi.org/10.1371/journal.pone.0196890.

Clow, L.A., Gross, P.S., Shih, C.S., Smith, L.C., 2000. Expression of SpC3, the sea urchin complement component, in response to lipopolysaccharide. Immunogenetics 51, 1021–1033. https://doi.org/10.1007/s002510000233.

Clow, L.A., Raftos, D.A., Gross, P.S., Smith, L.C., 2004. The sea urchin complement homologue, SpC3, functions as an opsonin. J. Exp. Biol. 207, 2147–2155. https://doi.org/10.1242/jeb.01001.

Coates, C.J., McCulloch, C., Betts, J., Whalley, T., 2017. Echinochrome A release by red spherule cells is an iron-withholding strategy of sea urchin innate immunity. J. Innate. Immun. 10, 119–130. https://doi.org/10.1159/000484722.

Dheilly, N.M., Birch, D., Nair, S.V., Raftos, D.A., 2011. Ultrastructural localization of highly variable 185/333 immune response proteins in the coelomocytes of the sea urchin, *Heliocidaris erythrogramma*. Immunol. Cell Biol. 89, 861–869. https://doi.org/10.1038/icb.2011.3.

Edds, K.T., 1977. Dynamic aspects of filopodial formation by reorganization of microfilaments. J. Cell Biol. 73, 479–491. https://doi.org/10.1083/jcb.73.2.479.

Edds, K.T., 1979. Isolation and characterization of two forms of a cytoskeleton. J. Cell Biol. 88, 109–115. https://doi.org/10.1083/jcb.83.1.109.

Edds, K.T., 1993. Cell biology of echinoid coelomocytes: I. Diversity and characterization of cell types. J. Invertebr. Pathol. 61, 173–178. https://doi.org/10.1006/jipa.1993.1031.

Engelmann, P., Hayashi, Y., Bodó, K., Ernszt, D., Somogyi, I., Steib, A., Orbán, J., Pollák, E., Nyitrai, M., Németh, P., Molnár, L., 2016. Phenotypic and functional characterization of earthworm coelomocyte subsets: linking light scatter-based cell typing and imaging of the sorted populations. Dev. Comp. Immunol. 65, 41–52. https://doi.org/10.1016/j.dci.2016.06.017.

Golconda, P., Buckley, K.M., Reynolds, C.R., Romanello, J.P., Smith, L.C., 2019. The axial organ and the pharynx are sites of hematopoiesis in the sea urchin. Front. Immunol. 10, 870. https://doi.org/10.3389/fimmu.2019.00870.

Gross, P.S., Clow, L.A., Smith, L.C., 2000. SpC3, the complement homologue from the purple sea urchin, *Strongylocentrotus purpuratus*, is expressed in two subpopulations of the phagocytic coelomocytes. Immunogenetics 51, 1034–1044. https://doi.org/10.1007/s002510000234.

Guerinot, M.L., West, P.A., Lee, J.V., Colwell, R.R., 1982. *Vibrio diazotrophicus* sp. nov., a marine nitrogen-fixing bacterium. Int. J. Syst. Bacteriol. 32, 350–357.

Henson, J.H., Nesbitt, D., Wright, B.D., Scholey, J.M., 1992. Immunolocalization of kinesin in sea urchin coelomocytes. Association of kinesin with intracellular organelles. J. Cell Sci. 103, 309–320.

Henson, J.H., Svitkina, T.M., Burns, A.R., Hughes, H.E., MacPartland, K.J., Nazarian, R., Borisy, G.G., 1999. Two components of actin-based retrograde flow in sea urchin coelomocytes. Mol. Biol. Cell 10, 4075–4090. https://doi.org/10.1091/mbc.10.12.4075.

Hira, J., Wolfson, D., Andersen, A.J.C., Haug, T., Stensvåg, K., 2020. Autofluorescence mediated red spherulocyte sorting provides insights into the source of spinochromes in sea urchins. Sci. Rep. 10, 1149. https://doi.org/10.1038/s41598-019-57387-7.

Hyman, L.H., 1955. The Invertebrates: Echinodermata, the Coelomate Bilateria, 4. McGraw-Hill Book Company, Inc., New York NY.

Johnson, P.T., 1969. The coelomic elements of sea urchins (*Strongylocentrotus*) I. The normal coelomocytes; their morphology and dynamics in hanging drops. J. Invertebr. Pathol. 13, 25–41. https://doi.org/10.1016/0022-2011(69)90236-5.

Liao, W.-Y., Fugmann, S.D., 2017. Lectins identify distinct populations of coelomocytes in Strongylocentrotus purpuratus. PLoS One 12, e0187987. https://doi.org/10.1371/journal.pone.0187987.

Lun, C.M., Schrankel, C.S., Chou, H.Y., Sacchi, S., Smith, L.C., 2016. A recombinant Sp185/333 protein from the purple sea urchin has multitasking binding activities towards certain microbes and PAMPs. Immunobiology 221, 889–903. https://doi.org/10.1016/j.imbio.2016.03.006.

Majeske, A.J., Bayne, C.J., Smith, L.C., 2013a. Aggregation of sea urchin phagocytes is augmented in vitro by lipopolysaccharide. PLoS One 8, e61419. https://doi.org/10.1371/journal.pone.0061419.

Majeske, A.J., Oleksyk, T.K., Smith, L.C., 2013b. The *Sp185/333* immune response genes and proteins are expressed in cells dispersed within all major organs of the adult purple sea urchin. Innate Immun. 19, 569–587.

Majeske, A.J., Oren, M., Sacchi, S., Smith, L.C., 2014. Single sea urchin phagocytes express messages of a single sequence from the diverse *Sp185/333* gene family in response to bacterial challenge. J. Immunol. 193, 5678–5688. https://doi.org/10.4049/jimmunol.1401681.

Messer, L.I., Wardlaw, A.C., 1980. Separation of the coelomocytes of *Echinus esculentus* by density gradient centrifugation. In: Jangoux, M. (Ed.), Echinoderms: Present and Past. Proceedings of the European Colloquium on Echinoderms, Brussels. A.A. Balkema, Rotterdam, pp. pp319–323.

Monte, T.C.d.C., Chometon, T.Q., Bertho, A.L., de Moura, V.S., de Vasconcellos, M.C., Garcia, J., Ferraz-Nogueira, R., Maldonado Júnior, A., Faro, M.J., 2019. Changes in hemocytes of *Biomphalaria glabrata* infected with *Echinostoma paraensei* and exposed to glyphosate-based herbicide. J. Invertebr. Pathol. 160, 67–75. https://doi.org/10.1016/j.jip.2018.11.007.

Oren, M., Rosental, B., Hawley, T.S., Kim, G.Y., Agronin, J., Reynolds, C.R., Grayfer, L., Smith, L.C., 2019. Individual sea urchin coelomocytes undergo somatic immune gene diversification. Front. Immunol. 10, 1298. https://doi.org/10.3389/fimmu.2019.01298.

Pagliara, P., Canicattì, C., 1993. Isolation of cytolytic granules from sea urchin amoebocytes. Eur. J. Cell Biol. 60, 179–184.

Piryaei, F., Ghavam Mostafavi, P., Shahbazzadeh, D., Pooshang Bagheri, K., 2018. Cytological study of *Echinometra mathaei* (echinoidea: camarodonta: Echinometra), the Persian gulf Sea Urchin. Int. J. Aquat. Sci. 9, 77–84. https://doi.org/10.29252/ijaah.4.2.1.

Romero, A., Novoa, B., Figueras, A., 2016. Cell mediated immune response of the Mediterranean sea urchin *Paracentrotus lividus* after PAMPs stimulation. Dev. Comp. Immunol. 62, 29–38. https://doi.org/10.1016/j.dci.2016.04.018.

Service, M., Wardlaw, A.C., 1984. Echinochrome-A as a bactericidal substance in the coelomic fluid of *Echinus esculentus* (L.). Comp. Biochem. Physiol. B Biochem. Mol. Biol. 79, 161–165. https://doi.org/10.1016/0305-0491(84)90008-7.

Sherman, L.S., Schrankel, C.S., Brown, K.J., Smith, L.C., 2015. Extraordinary diversity of immune response proteins among sea urchins: nickel-isolated Sp185/333 proteins show broad variations in size and charge. PLoS One 10, e0138892. https://doi.org/10.1371/journal.pone.0138892.

Smith, V., 1981. The echinoderms. In: Ratcliffe, N.A., Rowley, A.F. (Eds.), Invertebrate Blood Cells. Academic Press, London, pp. 513–562.

Smith, L.C., Britten, R.J., Davidson, E.H., 1992. SpCoell: a sea urchin profilin gene expressed specifically in coelomocytes in response to injury. Mol. Biol. Cell 3, 403–414.

Smith, L.C., Britten, R.J., Davidson, E.H., 1995. Lipopolysaccharide activates the sea urchin immune system. Dev. Comp. Immunol. 19, 217–224.

Smith, L.C., Ghosh, J., Buckley, K.M., Clow, L.A., Dheilly, N.M., Haug, T., Henson, J.H., Li, C., Lun, C.M., Majeske, A.J., Matranga, V., Nair, S.V., Rast, J.P., Raftos, D.A., Roth, M., Sacchi, S., Schrankel, C.S., Stensvåg, K., 2010. Echinoderm immunity. In: Söderhäll, K. (Ed.), Invertebrate Immunity. Springer Science+Business Media, LLC, Landes Bioscience, Austin TX, pp. 260–301. In: Advances in Experimental Medicine and Biology, 708.

Smith, L.C., Arizza, V., Barela Hudgell, M.A., Barone, G., Bodnar, A.G., Buckley, K.M., Cunsolo, V., Dheilly, N.M., Franchi, N., Fugmann, S.D., Furukawa, R., Garcia-Arraras, J., Henson, J.H., Hibino, T., Irons, Z.H., Li, C., Lun, C.M., Majeske, A.J., Oren, M., Pagliara, P., Pinsino, A., Raftos, D.A., Rast, J.P., Samasa, B., Schillaci, D., Schrankel, C.S., Stabili, L., Stensväg, K., Sutton, E., 2018. Echinodermata: the complex immune system in echinoderms. In: Cooper, E.L. (Ed.), Advances in Comparative Immunology. Springer International Publishing, pp. 409–501. https://doi.org/10.1007/978-3-319-76768-0_13.

Smith, L.C., Hawley, T.S., Henson, J.H., Majeske, A.J., Oren, M., Rosental, B., 2019. Methods for collection, handling, and analysis of sea urchin coelomocytes. In: Foltz, K.A., Hamdoun, A. (Eds.), Echinoderms. Methods in Cell Biology 150A, pp. 357–389. https://doi.org/10.1016/bs.mcb.2018.11.009.

Terwilliger, D.P., Buckley, K.M., Brockton, V., Ritter, N.J., Smith, L.C., 2007. Distinctive expression patterns of *185/333* genes in the purple sea urchin, *Strongylocentrotus purpuratus*: an unexpectedly diverse family of transcripts in response to LPS, β-1,3-glucan, and dsRNA. BMC Mol. Biol. 8, 16. https://doi.org/10.1186/1471-2199-8-16.

Wang, Y., Meng, S., Zhang, J., Ding, J., Li, Q., 2018. Production, characterization and application of monoclonal antibodies to the coelomocytes of sea urchin *Strongylocentrotus intermedius*. Fish Shellfish Immunol. 75, 301–307. https://doi.org/10.1016/j.fsi.2018.01.048.

Yui, M.A., Bayne, C.J., 1983. Echinoderm immunology: bacterial clearance by the sea urchin *Strongylocentrotus purpuratus*. Biol. Bull. 165, 473–486.